



Mapping and spatiotemporal dynamics of land-use and land-cover change based on the Google Earth Engine cloud platform from Landsat imagery: A case study of Zhoushan Island, China

Chao Chen^a, Xuebing Yang^b, Shenghui Jiang^{c,*}, Zhisong Liu^{b,d}

^a School of Geography Science and Geomatics Engineering, Suzhou University of Science and Technology, Suzhou, 215009, PR China

^b School of Information Engineering, Zhejiang Ocean University, Zhoushan, 316022, PR China

^c Key Lab of Submarine Geosciences and Prospecting Techniques, MOE and College of Marine Geoscience, Ocean University of China, Qingdao, 266100, PR China

^d Key Laboratory of Oceanographic Big Data Mining and Application of Zhejiang Province, Zhejiang Ocean University, Zhoushan, 316022, PR China

ARTICLE INFO

Keywords:

Zhoushan island
Landsat
GEE
Land use and land cover change
Spatio-temporal characteristics

ABSTRACT

Land resources are an essential foundation for socioeconomic development. Island land resources are limited, the type changes are particularly frequent, and the environment is fragile. Therefore, large-scale, long-term, and high-accuracy land-use classification and spatiotemporal characteristic analysis are of great significance for the sustainable development of islands. Based on the advantages of remote sensing indices and principal component analysis in accurate classification, and taking Zhoushan Archipelago, China, as the study area, in this work long-term satellite remote sensing data were used to perform land-use classification and spatiotemporal characteristic analysis. The classification results showed that the land-use types could be exactly classified, with the overall accuracy and Kappa coefficient greater than 94% and 0.93, respectively. The results of the spatiotemporal characteristic analysis showed that the built-up land and forest land areas increased by 90.00 km² and 36.83 km², respectively, while the area of the cropland/grassland decreased by 69.77 km². The areas of the water bodies, tidal flats, and bare land exhibited slight change trends. The spatial coverage of Zhoushan Island continuously expanded toward the coast, encroaching on nearby sea areas and tidal flats. The cropland/grassland was the most transferred-out area, at up to 108.94 km², and built-up land was the most transferred-in areas, at up to 73.31 km². This study provides a data basis and technical support for the scientific management of land resources.

1. Introduction

Land resources are necessary for human survival and development, and it is crucial to improve sustainable development and the cognition of human–land relationships. Land-use/cover changes are an important source of information for understanding the complex interactions between human activities and the environment [1–4]. Large-scale, long-term, and high-accuracy land-use data are of great significance to the study of long-term temporal and spatial land-use changes [4–8]. An island is a compound area that contains marine resources and environments, with a relatively simple geographic structure, a limited environmental capacity, poor stability, and a

* Corresponding author.

E-mail address: jsh254677@ouc.edu.cn (S. Jiang).

<https://doi.org/10.1016/j.heliyon.2023.e19654>

Received 9 June 2023; Received in revised form 29 August 2023; Accepted 29 August 2023

Available online 4 September 2023

2405-8440/© 2023 The Authors. Published by Elsevier Ltd. This is an open access article under the CC BY-NC-ND license (<http://creativecommons.org/licenses/by-nc-nd/4.0/>).

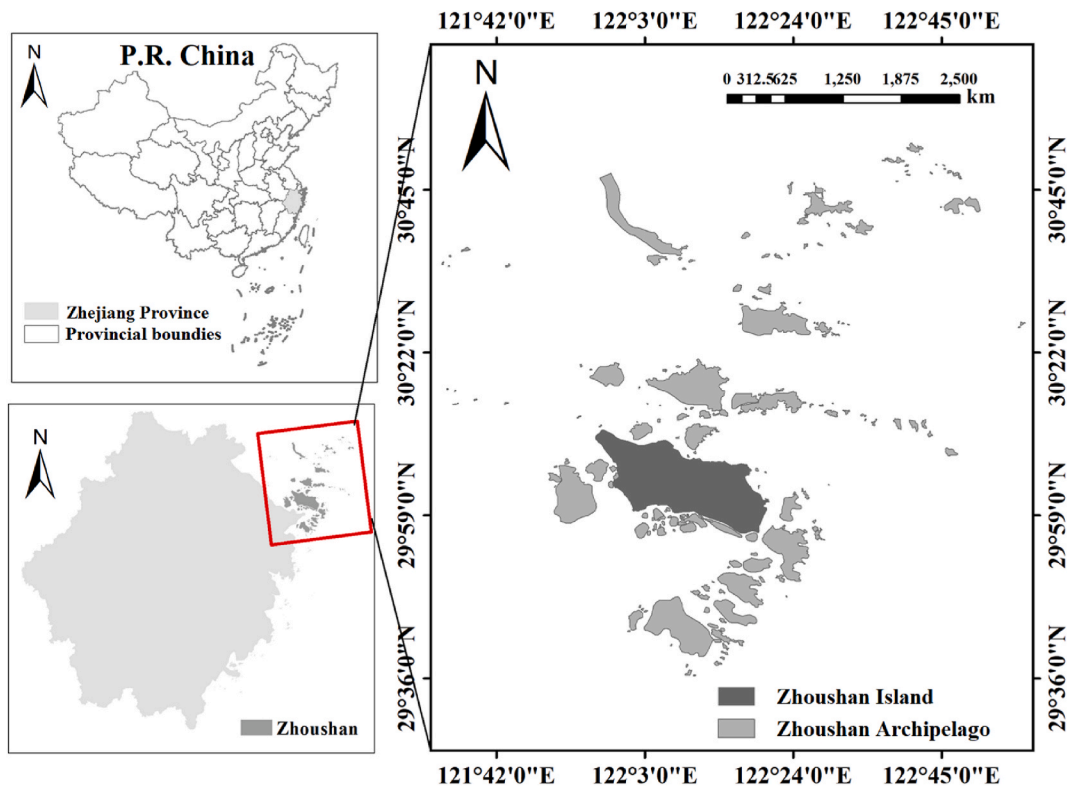


Fig. 1. Location of Zhoushan island.

comparatively fragile environment. Understanding land-use/cover change is a crucial precondition for conducting island ecological protection [9–11].

Land-use/cover change mapping based on traditional classifiers takes a long time and is less effective. These methods include the minimum distance classifier, maximum likelihood classifier, K-nearest neighbor classifier, K-means classifier, and ISODATA classifier, which has extremely high requirements for post-processing and other work [11–13]. In recent years, machine learning algorithms have been widely used in object recognition and remote sensing information extraction due to their powerful adaptive and self-learning parallel information processing capabilities [14–16]. Among them, the artificial neural network, decision tree, support vector machine, and random forest (RF) algorithm show good classification effect, and have received increasing attention from researchers [17–20].

Researchers in China and abroad have investigated machine learning classification algorithms in terms of research areas, data sources, and classification algorithms with the help of remote sensing technologies. The research areas have included provinces, river basins, and nations. For example, Shi et al. took Jiangsu Province as the research area and analyzed the historical evolution of land use in Jiangsu Province from 1990 to 2010 [21]. Yang et al. discussed the evolution characteristics of land-use/cover changes in the Yellow River Basin from 2000 to 2020 [22]. Alijani et al. studied the evolution characteristics of land-use/cover changes in Iran over 20 years, from 1996 to 2016 [23]. The data sources used in previous studies include hyperspectral, light detection and ranging (Lidar), moderate resolution imaging spectroradiometer (MODIS) data, and Landsat data [24–27]. Classification algorithms include the 2-D convolutional neural network, hybrid convolutional network, and RF [28–30]. Remote sensing indices can highlight a certain type of ground object, such as the normalized difference vegetation index (NDVI), normalized difference water index (NDWI), and normalized difference built-up index (NDBI). Therefore, many researchers have added indices to improve classification accuracy.

Different from land areas, islands have the characteristics of limited land resources, frequent changes of land-use types, and high landscape fragmentation. Therefore, it is necessary to use multiple indicators to conduct the large-scale, long-term, high-accuracy analysis of the spatiotemporal characteristics of island land use. Considering the advantages of remote sensing indices and principal component analysis in accurate classification, in this study an RF classification algorithm was developed based on remote sensing indices and principal component analysis. The spatiotemporal characteristics of the land-use/cover change on Zhoushan Island were analyzed based on long-term satellite remote sensing data.

Table 1
Landsat satellite image data used.

Imaging time	Satellite	Sensor	Spatial resolution	Bands
1985/01/01–1985/12/31	Landsat5	Thematic mapper (TM)	30 m	Band 1: blue (0.45–0.52 μm)
1990/01/01–1990/12/31				Band 2: green (0.52–0.60 μm)
1995/01/01–1995/12/31				Band 3: red (0.63–0.69 μm)
2000/01/01–2000/12/31				Band 4: near-infrared (0.76–0.90 μm)
2005/01/01–2005/12/31				Band 5: near-infrared (1.55–1.75 μm)
2010/01/01–2010/12/31				Band 7: mid-infrared (2.08–2.35 μm)
2015/01/01–2015/12/31	Landsat8	Operational land imager (OLI)	30 m	Band 1: coastal aerosol (0.43–0.45 μm)
2020/01/01–2020/12/31				Band 2: blue (0.450–0.51 μm)
				Band 3: green (0.53–0.59 μm)
				Band 4: red (0.64–0.67 μm)
				Band 5: near-infrared (0.85–0.88 μm)
				Band 6: SWIR 1 (1.57–1.65 μm)
		Band 7: SWIR 2 (2.11–2.29 μm)		Band 9: cirrus (1.36–1.38 μm)
2022/01/01–2022/12/31	Landsat9	OLI-2	30 m	Band 1: coastal aerosol (0.43–0.45 μm)
				Band 2: blue (0.450–0.51 μm)
				Band 3: green (0.53–0.59 μm)
				Band 4: red (0.64–0.67 μm)
				Band 5: near-infrared (0.85–0.88 μm)
				Band 6: SWIR 1 (1.57–1.65 μm)
				Band 7: SWIR 2 (2.11–2.29 μm)
				Band 9: cirrus (1.36–1.38 μm)

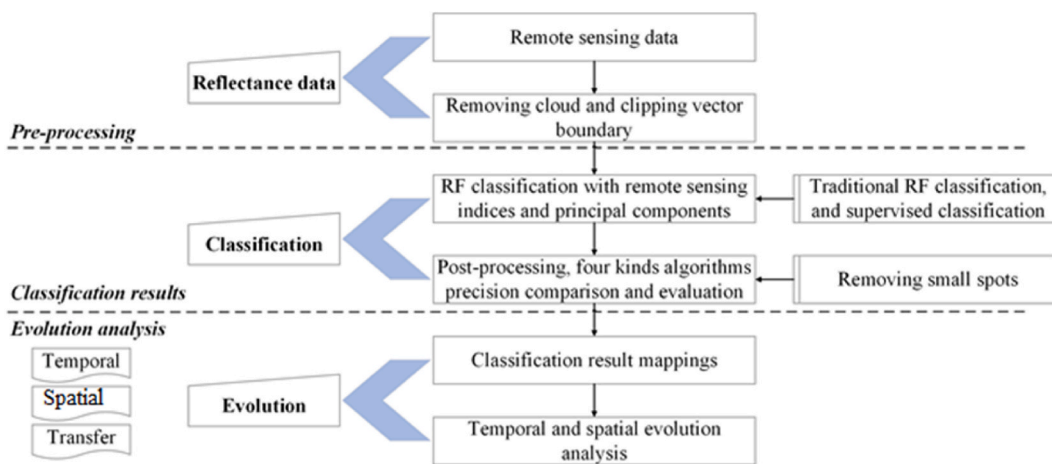


Fig. 2. Flow chart of spatiotemporal pattern evolution analysis.

2. Study area and data sources

2.1. Study area

Zhoushan City is the first provincial prefecture-level city organized as an archipelago in China. It is located in the northeastern part of Zhejiang Province and is bordered by the East China Sea to the east, Hangzhou Bay to the west, and Shanghai to the north. In the present study, Zhoushan Island, the largest island in Zhejiang Province, was selected as the research area. Zhoushan Island has an area of approximately 503 km² [31]; its location is shown in Fig. 1.

2.2. Data

In this study, Landsat5, Landsat8, and Landsat9 satellite remote sensing images in nine time periods (1985, 1990, 1995, 2000, 2005, 2010, 2015, 2020, and 2022) provided by the Google Earth Engine (GEE) cloud platform were used for land-use classification [32]. The Landsat satellites are among the optical remote sensing satellite series with the longest operating time in orbit for investigating land resources and drawing various thematic maps [33–35]. The details are presented in Table 1.

Table 2
Land-use types and performance characteristics.

Classification	Secondary feature categories	Visual characteristics
Built-up land	Urban and rural residential land, industrial land, traffic land	
Forest land	Woods, shrubs, and orchards	
Cropland/grassland	Fields, grassland, and other agricultural land	
Water bodies	Water land, breeding ponds, and water conservancy facilities	
Tidal flats	Tidal flats, salt pans, and aquaculture land	
Bare land	Bare soil, bare mountains, and other undeveloped land	

3. Research methods

Based on the advantages of the remote sensing indices and principal component analysis for accurate classification, this study was based on the characteristics of the study area, the classification of the remote sensing images, and the spatiotemporal characteristic analysis of the land-use/cover changes from 1985 to 2022. A flowchart of this study is shown in Fig. 2.

First, the Landsat satellite remote sensing images covering the study area were obtained from the GEE. Second, the image stacks were constructed based on the original remote sensing images, multi-feature indices, and principal components. Then, remote sensing image classification was implemented based on the RF algorithm. Finally, the spatiotemporal characteristics were explored from three perspectives: area changes, spatial variations, and land-use transfers.

3.1. Data pre-processing

The remote sensing data from the Landsat5, Landsat8, and Landsat9 satellites were preprocessed to remove the cloud pixels and clip the boundary in the image collection of each time phase in the study area [36–40]. The process was as follows. First, the products of the Landsat 5 (United States Geological Survey (USGS) Landsat 5 Surface Reflectance Tier 1), Landsat8 (USGS Landsat 8 Surface Reflectance Tier 1), and Landsat9 (USGS Landsat 9 Level 2, Collection 2, Tier 1) were input to the GEE, including all of the coverage areas in 1985, 1990, 1995, 2000, 2005, 2010, 2015, 2020, and 2022, and the preprocessed surface reflectance data were obtained. Then, an initial dense time series image collection of the study area was established. Second, pixels with poor observation quality, such as clouds and shadows, were removed using the QA band in GEE, and then, inter-annual composite images were obtained using the median filter method. Finally, the codes were run in GEE to cut out the boundary of Zhoushan Island.

3.2. Determination of land-use categories

The ground objects in the study area were considered relatively discrete and limited by the spatial resolution [41]. Based on the land-use documents issued by relevant departments, the land-use types were integrated into six categories: built-up land, forest land, cropland/grassland, water bodies, tidal flats, and bare land. The details are presented in Table 2.

Table 3
Formulas for remote sensing indices.

Indices	Formula	References
Normalized difference vegetation index	$NDVI = \frac{(NIR - R)}{(NIR + R)}$	[37,40]
Ratio vegetation index	$RVI = \frac{NIR}{R}$	[41]
Enhanced vegetation index	$EVI = 2.5 * \frac{NIR - RED}{(NIR + 6 * RED - 7.5 * BLUE + 1)}$	[38,42]
Difference vegetation index	$DVI = NIR - R$	[39,43]
Normalized difference water index	$NDWI = \frac{(GREEN - NIR)}{(GREEN + NIR)}$	[44,45]
Normalized difference building vegetation index	$NDBI = \frac{(SWIR - NIR)}{(SWIR + NIR)}$	[45]
Regulated soil vegetation index	$SAVI = \frac{(NIR - RED) * (1 + 0.5)}{(NIR + RED + 0.5)}$	[46]
Urban building index	$IBI_A = \frac{2 * SWIR1}{SWIR1 + NIR}$ $IBI_B = \frac{NIR}{(NIR + RED)} + \frac{GREEN}{(GREEN + SWIR1)}$ $IBI = \frac{IBI_A - IBI_B}{IBI_A + IBI_B}$	[47,48]

3.3. Remote sensing image classification based on the RF algorithm

The training samples were selected according to the principles of randomness and uniformity. Based on the traditional RF algorithm, in this study, land-use classification via the integration of remote sensing indices (the NDVI, ratio vegetation index, enhanced vegetation index, difference vegetation index (DVI), NDWI, NDBI, regulated soil vegetation index (SAVI), and urban building index (UBI)) and the first, second, and third components was implemented. The remote sensing indices are described in Table 3.

3.4. Accuracy evaluation

The confusion matrix is used to judge whether the objects in each category are correctly classified by comparing the position and category of the measured pixels with the corresponding position and category in the classification results. The specific evaluation indicators incorporate the overall accuracy (OA) and the Kappa coefficient. The OA represents the ratio of the number of correctly classified pixels to the total number of pixels. The Kappa coefficient is an index that measures the degree of agreement between the classification results and the real data. Not only the correctly classified pixels, but also the missed and misclassified pixels are considered. The expressions of the OA and the Kappa coefficient are

$$\left\{ \begin{aligned} p &= \frac{\sum_{i=1}^n x_{ii}}{\sum_{j=1}^n \sum_{i=1}^n x_{ij}} \\ K &= \frac{N \sum_{i=1}^n x_{ii} - \sum (x_{i+} \times x_{+i})}{N^2 - \sum (x_{i+} \times x_{+i})} \end{aligned} \right. \tag{1}$$

where x_{i+} , x_{+i} , x_{ii} describe the element in a certain row, column, and diagonal of the confusion matrix, respectively; and N is the total number of pixels. Therefore, the larger the OA and Kappa coefficient are, the higher the accuracy of the results is [49,50].

4. Results and analysis

4.1. Land-use classification results

The post-processing of the classification results mainly removed the spots caused by image noise and the classification algorithm, and mapping was conducted using the ArcGIS platform. The maps of land-use and land-cover change of Zhoushan island from 1985 to 2022 are shown in Fig. 3.

It can be seen from Fig. 3 that the classification results of the RF algorithm, which integrates the remote sensing indices and the principal components, are accurate, and the boundaries between ground objects are clear. The built-up land, forest land, cropland/grassland, water bodies, tidal flats, and bare land are distinguished, and misclassifications are rare. The OA and Kappa coefficient of the traditional RF classification algorithm using only the reflectance bands, support vector machine classification, and minimum distance classification [51–54] are shown in Table 4 and Table 5, respectively.

It can be seen from Tables 4 and 5 that the OA and Kappa coefficient of the algorithm are greater than 94% and 0.93, respectively,

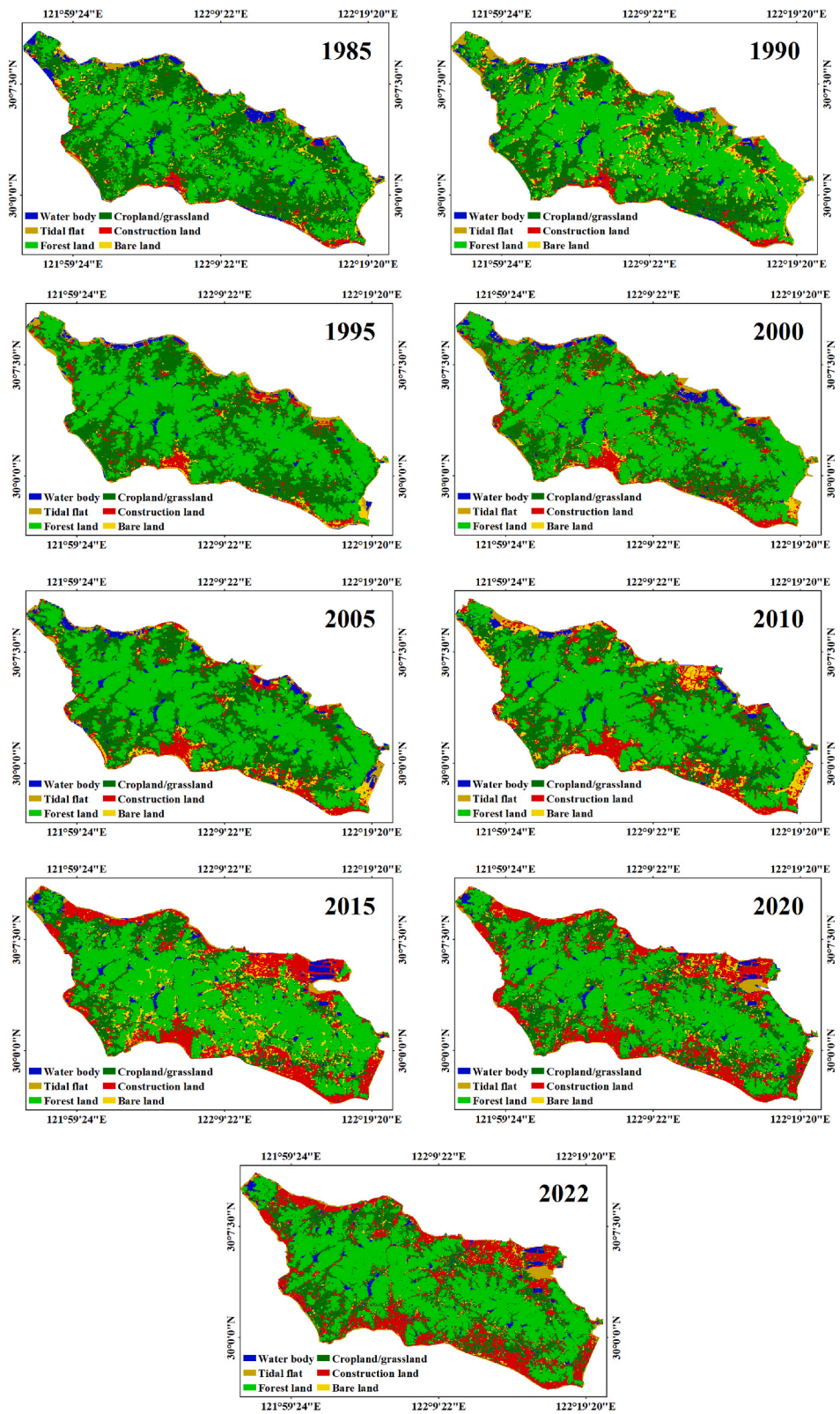


Fig. 3. Classification result maps.

Table 4
List of OA values.

	RF of indices and PCA	RF of reflectance alone	Support vector machines	Minimum distance
1985	95.35%	93.00%	91.50%	84.00%
1990	98.40%	96.17%	93.99%	92.90%
1995	96.07%	94.22%	83.58%	84.39%
2000	98.68%	96.45%	95.74%	90.07%
2005	97.18%	96.34%	90.24%	93.29%
2010	97.16%	95.68%	92.97%	84.86%
2015	98.34%	93.29%	62.20%	90.24%
2020	94.78%	93.48%	73.91%	84.35%
2022	95.83%	94.38%	93.98%	91.57%

Table 5
List of Kappa coefficients.

	RF of indices and PCA	RF of reflectance alone	Support vector machine	Minimum distance
1985	0.94	0.91	0.89	0.80
1990	0.98	0.95	0.93	0.91
1995	0.95	0.93	0.80	0.81
2000	0.98	0.96	0.95	0.88
2005	0.96	0.95	0.88	0.92
2010	0.97	0.95	0.92	0.82
2015	0.98	0.92	0.53	0.88
2020	0.93	0.92	0.67	0.81
2022	0.95	0.93	0.92	0.90

Table 6
Area of each land-use type (km²).

Year	Built-up land	Cropland/grassland	Forest land	Water bodies	Tidal flats	Bare land	Total
1985	19.89	211.22	199.11	20.14	11.56	24.39	486.31
1990	26.50	163.15	220.72	18.34	18.43	40.54	487.69
1995	28.41	170.99	249.83	10.88	20.44	10.96	491.52
2000	44.99	119.22	280.53	17.76	17.00	15.00	494.50
2005	51.01	148.72	250.77	16.63	15.04	14.59	496.76
2010	61.00	140.78	248.99	13.28	9.32	31.55	504.91
2015	100.98	108.85	244.80	15.59	10.52	42.05	522.79
2020	105.63	139.37	231.58	13.04	10.75	23.70	524.07
2022	109.89	141.45	235.94	12.18	14.57	13.63	527.65

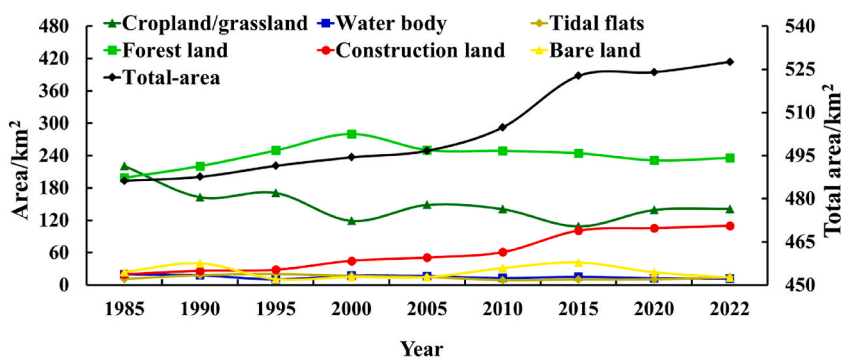


Fig. 4. Land-use category areas in different years.

with average values of 96.87% and 0.96, respectively. These values are significantly higher than those of the traditional RF classification algorithm that uses only reflectance bands, support vector machine classification, and minimum distance classification. In conclusion, this algorithm had high classification accuracy and a better classification effect, and it was used for the subsequent analysis.

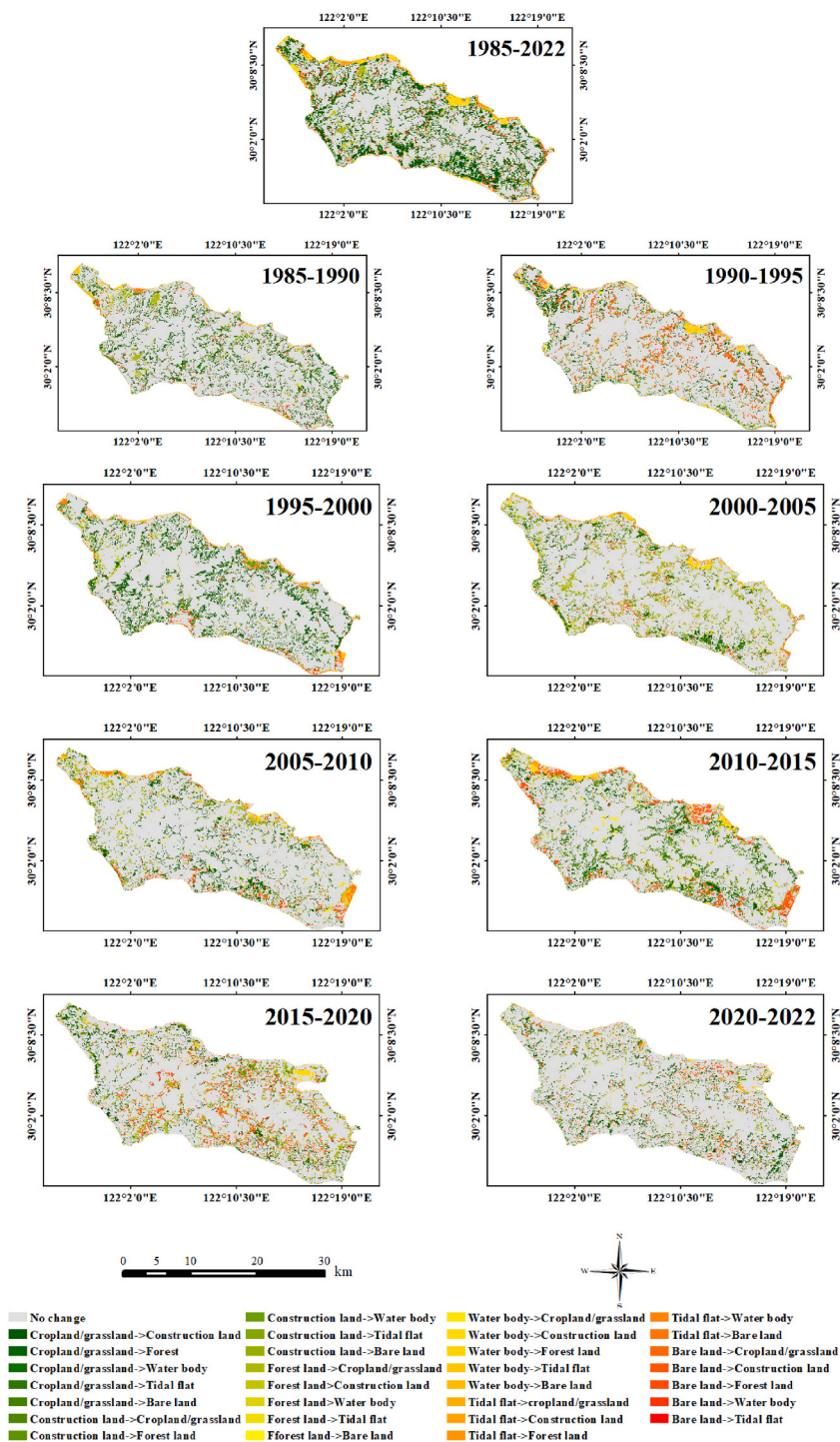


Fig. 5. Spatial distribution maps of land-use type transfer.

4.2. Analysis of spatiotemporal characteristics

4.2.1. Analysis of area change of land-use types

The area change refers to changes in the areas of the land-use types over time, which can reflect the intensities of the land-use types [55–57]. The areas and area variations of each land-use type in different years were counted (Table 6 and Fig. 4).

It can be seen from Table 6 and Fig. 4 that the total land area of Zhoushan Island changed from 486.31 km² to 527.65 km²,

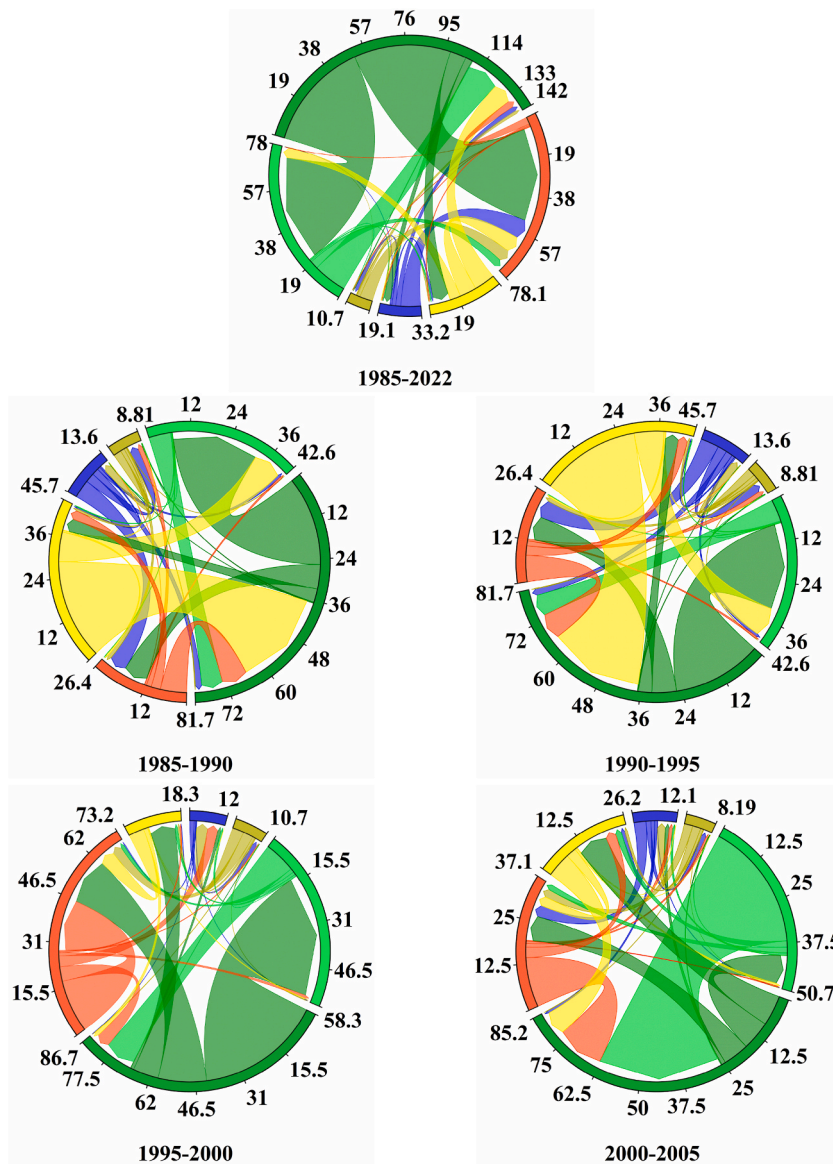


Fig. 6. Land-use type transfer chord diagrams.

increasing by 41.34 km² due to the reclamation of marine areas, and the built-up land, forest land, and cropland/grassland exhibited obvious change trends. The built-up land area steadily increased from 19.89 km² in 1985 to 109.89 km² in 2022, with an average annual increase of 2.43 km²/a and an average rate of increase of 12.23%. The forest land area increased from 199.11 km² in 1985 to 235.94 km² in 2022, an increase of 36.83 km², with an average annual increase of 1.00 km²/a and an average rate of increase of 0.50%. The area of the cropland/grassland significantly decreased from 211.22 km² in 1985 to 141.45 km² in 2022, a decrease of 69.77 km², with an average annual decrease of 1.89 km²/a and an average rate of decrease of 0.89%. The areas of the water bodies, tidal flats, and bare land exhibited slight change trends. The water body area decreased by 7.96 km², the bare land area decreased by 10.76 km², and the tidal flat area increased by 3.01 km² over the past 37 years.

4.2.2. Spatial variation analysis

Spatial change refers to the transfer of land-use types, which is necessary for clarifying the characteristics and laws of the transitions between land-use types during various periods [58–60]. Transfer maps of the land-use types for different periods were created to visualize the spatial variation distributions, as shown in Figs. 5 and 6.

Figs. 5 and 6 show that the changes in the spatial coverage of the built-up land, forest land, and cropland/grassland were the most obvious from 1985 to 2022. The spatial coverage of the built-up land increased, mainly through encroaching on cropland/grassland.

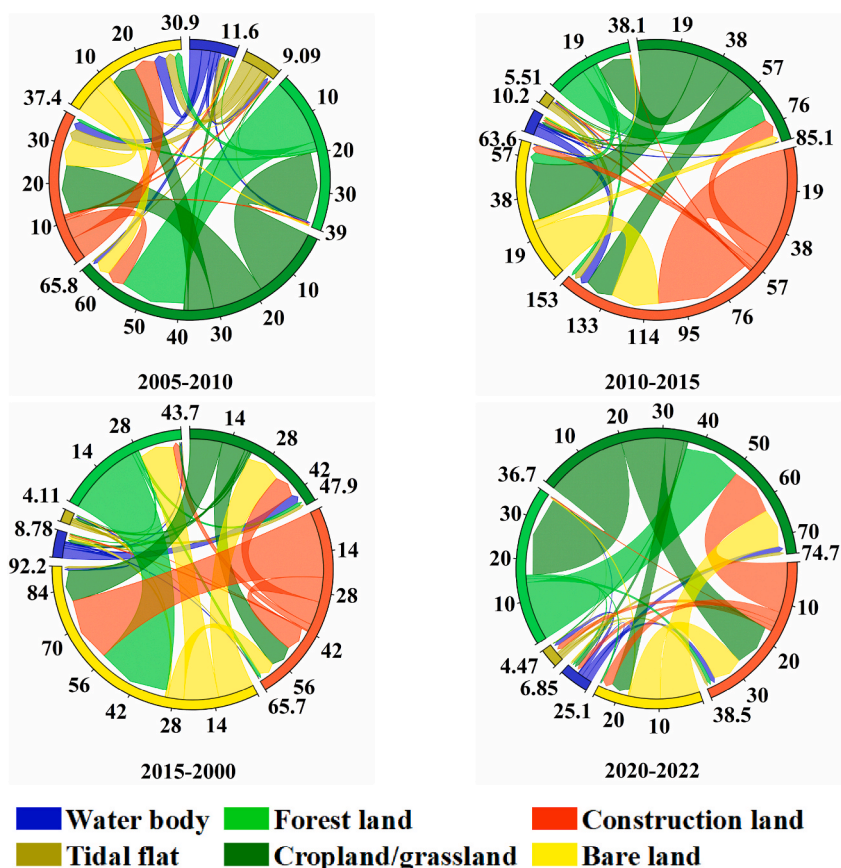


Fig. 6. (continued).

Table 7
Land-use transfer matrix for 1985–2022 (km²).

		2022						Total area in 1985
		Built-up land	Forest land	Cropland/grassland	Water bodies	Tidal flats	Bare land	
1985	Built-up land	15.06	0.16	3.34	0.41	0.33	0.55	19.85
	Forest land	3.82	177.96	15.90	0.53	0.10	0.79	199.10
	Bare land	7.96	4.95	9.93	0.18	0.02	1.35	24.39
	Cropland/grassland	46.03	51.60	102.27	3.20	0.40	7.71	211.21
	Water bodies	9.39	0.15	2.38	4.90	1.82	0.83	19.47
	Tidal flats	6.11	0.01	1.41	0.21	2.49	0.32	10.55
Total area in 2022		88.37	234.83	135.23	9.43	5.16	11.55	484.57

The main transfer areas were Baiquan Town, Dinghai District, Putuo District, Donggang, and Diaomen Port. The forest land and cropland/grassland were transformed into each other, but the area converted from cropland/grassland to forest land was much larger, resulting in the expansion of the spatial range of the forest land. Due to the double erosion through conversion to built-up land and forest land, the spatial coverage of the cropland/grassland was reduced. The main transfer areas were Shijiao Township, Qianlan Township, and Zhanmao Township. The changes in the spatial coverage of the water bodies, tidal flats, and bare land were small. Among them, the water bodies were mainly eroded by built-up land, and the bare land was mainly encroached upon by forest land, built-up land, and cropland/grassland. The tidal flats were mainly distributed near the boundary of Zhoushan Island, and although it was transferred out more, the overall spatial coverage of the tidal flats increased through expansion toward the coast.

4.2.3. Transfer of land-use types

The land-use transfer matrix can directly reflect changes in the land-use types and quantities [61–63]. The area transfer situations of the land-use types from 1985 to 2022 are recorded in Table 7. The rows express the transfer-out compositions of the land-use types in 1985, and the columns denote the transfer-in compositions of land-use types in 2022.

As shown in Table 7, the cropland/grassland was the most transferred-out area, with up to 108.94 km² transferred out, and built-up

land was the most transferred-in area, with up to 73.31 km² transferred in. The main types of cropland/grassland transfers were forest land and built-up land, with areas of 51.60 km² and 46.03 km² transferred from 1985 to 2022, respectively. The main pattern of built-up land expansion was the occupation of cropland/grassland. From 1985 to 2020, a total 46.03 km² of cropland/grassland was transferred to built-up land, accounting for 52.09% of all transferred areas.

5. Discussion and conclusions

Based on traditional RF classification, supervised classification, and machine learning classification algorithms, and considering the advantages of remote sensing indices and principal component analysis in accurate classification, an RF algorithm that integrates remote sensing indices and principal component analysis was developed. Then, the spatiotemporal characteristics of the land-use types were analyzed based on a long-term sequence of satellite remote sensing data. The main contributions of this study are as follows.

- (1) The classification algorithm can accurately classify land-use types, and the mean values of the OA and Kappa coefficients are 96.87% and 0.96, respectively. This indicates that the proposed method can obtain more accurate land-use/cover change information.
- (2) The built-up land area continuously increased by 90 km² over the past 37 years. The forest land and cropland/grassland areas changed significantly. The forest land area increased by 36.83 km², and the cropland/grassland area decreased by 69.77 km². The water body, tidal flat, and bare land areas exhibited slight increasing and decreasing trends.
- (3) The built-up land was mainly increased through encroachment on cropland/grassland, and these changes were concentrated in Baiquan Town, Dinghai District, Putuo District, Donggang, and Diaomen Port. The forest land and cropland/grassland were transferred into each other, and the spatial coverage of the forest land increased, while that of the cropland/grassland decreased due to its double erosion by built-up land and forest land. This mainly occurred in Shijiao Township, Qianlan Township, and Zhanmao Township.
- (4) The transfer-in and transfer-out areas of the built-up land, forest land, and cropland/grassland were relatively evident, and the cropland/grassland was mainly occupied by built-up land and forest land over the past 37 years. The transfer of the water body, tidal flat, and bare land areas was relatively small, and they were mainly occupied by built-up land, forest land, and cropland/grassland.

Future investigations will focus on: (1) high-resolution regional data, with the combination of high-precision algorithms to conduct land-use classification to obtain more accurate land-use type information; and (2) the establishment of evaluation patterns for spatiotemporal characteristics.

Author contribution statement

Chao Chen: Conceived and designed the experiments; Performed the experiments; Analyzed and interpreted the data; Wrote the paper.

Xuebing Yang: Conceived and designed the experiments; Performed the experiments; Wrote the paper.

Shenghui Jiang and Zhisong Liu: Analyzed and interpreted the data.

Data availability statement

Data will be made available on request.

Declaration of competing interest

The authors declare that they have no known competing financial interests or personal relationships that could have appeared to influence the work reported in this paper.

Acknowledgments

The authors would like to thank the editors and the anonymous reviewers for their outstanding comments and suggestions, which greatly helped improve the technical quality and presentation of this manuscript. We also thank the United States Geological Survey (www.usgs.gov), the National Aeronautics and Space Administration (www.nasa.gov), and the Chinese Academy of Science (www.ids.ceode.ac.cn) for the freely available Landsat remote sensing images. This work was supported by the National Natural Science Foundation of China (Grant No. 42171311). We thank LetPub (www.letpub.com) for linguistic assistance and pre-submission expert review.

References

- [1] G. Sun, Z. Pan, A. Zhang, X. Jia, J. Ren, H. Fu, K. Yan, Large kernel spectral and spatial attention networks for hyperspectral image classification, *IEEE Trans. Geosci. Rem. Sens.* 61 (2023) 5519915 (Early Access).

- [2] M. Irannezhad, B. Ahmadi, J. Liu, D. Chen, J.H. Matthews, Global water security: a shining star in the dark sky of achieving the sustainable development goals, *Sustainable Horizons* 1 (2022), 100005.
- [3] C. Chen, J. Liang, G. Yang, W. Sun, Spatio-temporal distribution of harmful algal blooms and their correlations with marine hydrological elements in offshore areas, China, *Ocean Coast Manag.* 238 (2023), 106554.
- [4] C. Chen, J. Liang, F. Xie, Z. Hu, W. Sun, G. Yang, J. Yu, J. Chen, L.H. Wang, L.Y. Wang, H.X. Chen, X.Y. He, Z. Zhang, Temporal and spatial variation of coastline using remote sensing images for Zhoushan archipelago, China, *Int. J. Appl. Earth Obs. Geoinf.* 107 (2022), 102711.
- [5] P. Potapov, M.C. Hansen, I. Komareddy, A. Komareddy, S. Turubanova, A. Picken, B. Adusei, A. Tyukavina, Q. Ying, Landsat analysis ready data for global land cover and land cover change mapping, #426, *Rem. Sens.* 12 (2020).
- [6] X. Hou, L. Feng, High-resolution satellite observations reveal extensive algal blooms in both small and large lakes in China, *Sustainable Horizons* 6 (2023), 100054.
- [7] M. Carey, J. Boland, G. Keppel, Habitat diversity, resource availability and island age in the species-area relationship, *J. Biogeogr.* 50 (2023) 767–779.
- [8] M. Lancia, Y. Yao, C.B. Andrews, X. Wang, X. Kuang, J. Ni, S.M. Gorelick, B.R. Scanlon, Y. Wang, C. Zheng, The China groundwater crisis: a mechanistic analysis with implications for global sustainability, *Sustainable Horizons* 4 (2022), 100042.
- [9] J. Ding, C. Feng, G. Ye, G. Zhong, L.M. Chou, X. Chen, M. Liu, Incorporating ecological values into the valuation system of uninhabited islands in China, *Int. J. Appl. Earth Obs. Geoinf.* 110 (2022), 102819.
- [10] Z. Xie, X. Li, Y. Chi, D. Jiang, Y. Zhang, Y. Ma, S. Chen, Ecosystem service value decreases more rapidly under the dual pressures of land use change and ecological vulnerability: a case study in Zhujiajian Island, *Ocean Coast Manag.* 201 (2021), 105493.
- [11] C. Zhang, J. Cheng, Q. Tian, Unsupervised and semi-supervised image classification with weak semantic consistency, *IEEE Trans. Multimed.* 21 (2019) 2482–2491.
- [12] J. Calvert, J.A. Strong, M. Service, C. McGonigle, R. Quinn, An evaluation of supervised and unsupervised classification techniques for marine benthic habitat mapping using multibeam echosounder data, *ICES (Int. Council. Explor. Sea) J. Mar. Sci.* 72 (2015) 1498–1513.
- [13] H.G. Kuma, F.E. Feyessa, T.A. Demissie, Land-use/land-cover changes and implications in Southern Ethiopia: evidence from remote sensing and informants, *Heliyon* 8 (2022), e09071.
- [14] F. Lv, M. Han, T. Qiu, Remote sensing image classification based on ensemble extreme learning machine with stacked autoencoder, *IEEE Access* 5 (2017) 9021–9031.
- [15] J. Zuo, L. Zhang, B. Chen, J. Liao, M. Hashim, D. Sutrisno, M.E. Hason, R. Mahmood, D.A. Sani, Assessment of coastal sustainable development along the maritime silk road using an integrated natural-economic-social (NES) ecosystem, *Heliyon* 9 (2023), e17440.
- [16] C. Chen, J. Fu, S. Zhang, X. Zhao, Coastline information extraction based on the tasseled cap transformation of Landsat-8 OLI images, *Estuarine, Coastal and Shelf Science* 217 (2019) 281–291.
- [17] H. Fu, G. Sun, L. Zhang, A. Zhang, J. Ren, X. Jia, F. Li, Three-dimensional singular spectrum analysis for precise land cover classification from UAV-borne hyperspectral benchmark datasets, *ISPRS J. Photogrammetry Remote Sens.* 203 (2023) 115–134.
- [18] H. Zhang, Z. Wang, J. Chai, Land use/cover change and influencing factors inside the urban development boundary of different level cities: a case study in Hubei Province, China, *Heliyon* 8 (2022) (2022), e10408.
- [19] T. Belay, T. Melese, A. Senamaw, Impacts of land use and land cover change on ecosystem service values in the Afroalpine area of Guna Mountain, Northwest Ethiopia, *Heliyon* 8 (2022) (2022), e12246.
- [20] W. Sun, K. Liu, G. Ren, W. Liu, G. Yang, X. Meng, J. Peng, A simple and effective spectral-spatial method for mapping large-scale coastal wetlands using China ZY1-02D satellite hyperspectral images, #102572, *Int. J. Appl. Earth Obs. Geoinf.* 104 (2021).
- [21] G. Shi, P. Ye, L. Ding, A. Quinones, Y. Li, N. Jiang, Spatio-temporal patterns of land use and cover change from 1990 to 2010: a case study of Jiangsu province, China, *Int. J. Environ. Res. Publ. Health* 16 (2019) 907.
- [22] R. Yang, H. Chen, S. Chen, Y. Ye, Spatiotemporal evolution and prediction of land use/land cover changes and ecosystem service variation in the Yellow River Basin, China, *Ecol. Indicat.* 145 (2022), 109579.
- [23] Z. Alijani, F. Hosseinali, A. Biswas, Spatio-temporal evolution of agricultural land use change drivers: a case study from Chalous region, Iran, #110326, *J. Environ. Manag.* 262 (2020).
- [24] H. Fu, G. Sun, A. Zhang, B. Shao, J. Ren, X. Jia, Tensor singular spectrum analysis for 3-D feature extraction in hyperspectral images, *IEEE Trans. Geosci. Rem. Sens.* 61 (2023), 5403914.
- [25] K. Feng, T. Wang, S. Liu, W. Kang, X. Chen, Z. Guo, Y. Zhi, Monitoring desertification using machine-learning techniques with multiple indicators derived from MODIS images in Mu Us Sandy Land, China, *Rem. Sens.* 14 (2022) 2663.
- [26] H. Chen, C. Chen, Z. Zhang, C. Lu, L. Wang, X. He, Y. Chu, J. Chen, Changes of the spatial and temporal characteristics of land-use landscape patterns using multi-temporal Landsat satellite data: a case study of Zhoushan Island, China, *Ocean Coast Manag.* 213 (2021), 105842.
- [27] S. Jia, Z. Zhan, M. Xu, Shearlet-based structure-aware filtering for hyperspectral and LiDAR data classification, *Journal of Remote Sensing* 2021 (2021), 9825415.
- [28] C. Wang, Y. Zhang, X. Wu, W. Yang, H. Qiang, B. Lu, J. Wang, R-Imnet, Spatial-temporal evolution analysis of resource-exhausted urban land based on residual-intelligent module network, *Rem. Sens.* 14 (2022) 2185.
- [29] O. Rozenstein, T. Paz-Kagan, C. Salbach, A. Karnieli, Comparing the effect of preprocessing transformations on methods of land-use classification derived from spectral soil measurements, *IEEE J. Sel. Top. Appl. Earth Obs. Rem. Sens.* 8 (2014) 2393–2404.
- [30] S. Gxokwe, T. Dube, D. Mazvimavi, Leveraging Google Earth Engine platform to characterize and map small seasonal wetlands in the semi-arid environments of South Africa, *Sci. Total Environ.* 803 (2022), 150139.
- [31] Y. Wu, T. Zhang, H. Zhang, T. Pan, X. Ni, A. Grydehoj, J. Zhang, Factors influencing the ecological security of island cities: a neighborhood-scale study of Zhoushan Island, China, *Sustain. Cities Soc.* 55 (2020), 102029.
- [32] M. Amani, A. Ghorbanian, S.A. Ahmadi, M. Kakoei, A. Moghimi, S.M. Mirmazloumi, S.H.A. Moghaddam, S. Mahdavi, M. Ghahremanloo, S. Parsian, Q. Wu, B. Brisco, Google earth engine cloud computing platform for remote sensing big data applications: a comprehensive review, *IEEE J. Sel. Top. Appl. Earth Obs. Rem. Sens.* 13 (2020) 5326–5350.
- [33] Z. Zhu, C.E. Woodcock, C. Holden, Z. Yang, Generating synthetic Landsat images based on all available Landsat data: predicting Landsat surface reflectance at any given time, *Rem. Sens. Environ.* 162 (2015) 67–83.
- [34] J.L. Dwyer, D.P. Roy, B. Sauer, C.B. Jenkerson, H.K. Zhang, L. Lyburner, Analysis ready data: enabling analysis of the Landsat archive, *Rem. Sens.* 10 (9) (2018) 1363.
- [35] M.J. Choate, R. Rengarajan, J.C. Storey, M. Lubke, Landsat 9 geometric characteristics using underfly data, *Rem. Sens.* 14 (15) (2022) 3781.
- [36] J. Yan, G. Zhang, H. Ling, F. Han, Comparison of time-integrated NDVI and annual maximum NDVI for assessing grassland dynamics, *Ecol. Indicat.* 136 (2022), 108611.
- [37] M. Jia, Z. Wang, D. Mao, C. Ren, K. Song, C. Zhao, C. Wang, X. Xiao, Y. Wang, (2023). Mapping Global Distribution of Mangrove Forests at 10-m Resolution, *Science Bulletin*, 2023.
- [38] A. Bhatia, P.L. Teo, M. Li, J.Y.B. Lee, M.X.J. Chan, T.W. Yeo, M. Mathur, S. Tagore, Yeo, S.H. George, S. Arulkumar, Dinoprostone vaginal insert (DVI) versus adjunctive sweeping of membranes and DVI for term induction of labor, *J. Obstet. Gynaecol. Res.* 47 (9) (2021) 3171–3178.
- [39] S. Manna, B. Raychaudhuri, Mapping distribution of Sundarban mangroves using Sentinel-2 data and new spectral metric for detecting their health condition, *Geocarto Int.* 35 (4) (2020) 434–452.
- [40] C. Zhao, M. Jia, Z. Wang, D. Mao, Y. Wang, Toward a better understanding of coastal salt marsh mapping: a case from China using dual-temporal images, *Rem. Sens. Environ.* 295 (2023), 113664.
- [41] E.E. Maeda, J. Heiskanen, L.E. Aragão, J. Rinne, Can MODIS EVI monitor ecosystem productivity in the Amazon rainforest? *Geophys. Res. Lett.* 41 (20) (2014) 7176–7183.

- [42] B. Franch, E.F. Vermote, S. Skakun, J.C. Roger, I. Becker-Reshef, E. Murphy, C. Justice, Remote sensing based yield monitoring: application to winter wheat in United States and Ukraine, *Int. J. Appl. Earth Obs. Geoinf.* 76 (2019) 112–127.
- [43] L. Chai, H. Jiang, W.T. Crow, S. Liu, S. Zhao, J. Liu, S. Yang, Estimating corn canopy water content from normalized difference water index (NDWI): an optimized NDWI-Based scheme and its feasibility for retrieving corn VWC, *IEEE Trans. Geosci. Rem. Sens.* 59 (10) (2020) 8168–8181.
- [44] K. Li, Y. Chen, A Genetic Algorithm-based urban cluster automatic threshold method by combining VIIRS DNB, NDVI, and NDBI to monitor urbanization, *Rem. Sens.* 10 (2) (2018) 277.
- [45] A. Nagy, A. Szabó, O.D. Adeniyi, J. Tamás, Wheat yield forecasting for the Tisza River catchment using landsat 8 NDVI and SAVI time series and reported crop statistics, *Agronomy* 11 (4) (2021) 652.
- [46] Y. Zhang, X. Ban, E. Li, Z. Wang, F. Xiao, Evaluating ecological health in the middle-lower reaches of the Hanjiang River with cascade reservoirs using the Planktonic index of biotic integrity (P-IBI), *Ecol. Indic.* 114 (2020), 106282.
- [47] T. Hou, W. Sun, C. Chen, G. Yang, X. Meng, J. Peng, Marine floating raft aquaculture extraction of hyperspectral remote sensing images based decision tree algorithm, *Int. J. Appl. Earth Obs. Geoinf.* 111 (2022), 102846.
- [48] A. Alem, S. Kumar, Deep learning models performance evaluations for remote sensed image classification, *IEEE Access* 10 (2022) 111784–111793.
- [49] W. Sun, Q. Du, Hyperspectral band selection: a review, *IEEE Geoscience and Remote Sensing Magazine* 7 (2) (2019) 118–139.
- [50] V.K. Rana, T.M.V. Suryanarayana, Performance evaluation of MLE, RF and SVM classification algorithms for watershed scale land use/land cover mapping using sentinel 2 bands, *Remote Sens. Appl.: Society and Environment* 19 (2020), 100351.
- [51] H. Yin, Y. Hu, M. Liu, C. Li, Y. Chang, Evolutions of 30-year spatio-temporal distribution and influencing factors of *Suaeda salsa* in Bohai Bay, China, *Rem. Sens.* 14 (1) (2022) 138.
- [52] X. Yang, S. Qiu, Z. Zhu, C. Rittenhouse, D. Riordan, M. Cullerton, Mapping understory plant communities in deciduous forests from Sentinel-2 time series, *Rem. Sens. Environ.* 293 (2023), 113601.
- [53] X. Yang, Z. Zhu, S. Qiu, K.D. Kroeger, Z. Zhu, S. Covington, S. Detection and characterization of coastal tidal wetland change in the northeastern US using Landsat time series, *Rem. Sens. Environ.* 276 (2022), 113047.
- [54] W. Sun, C. Chen, W. Liu, G. Yang, X. Meng, L. Wang, K. Ren, Coastline extraction using remote sensing: a review, *GIScience Remote Sens.* 60 (1) (2023), 2243671.
- [55] L. Jonathan, F. Adeline, L. Andyne, P. Céline, C. Hugues, Prediction of forest nutrient and moisture regimes from understory vegetation with random forest classification models, *Ecol. Indic.* 144 (2022), 109446.
- [56] M. Yang, C. Li, J. Guan, X. Yan, A supervised-learning p -norm distance metric for hyperspectral remote sensing image classification, *Geosci. Rem. Sens. Lett. IEEE* 15 (9) (2018) 1432–1436.
- [57] C. Chen, H. Chen, J. Liang, W. Huang, W. Xu, B. Li, J. Wang, Extraction of water body information from remote sensing imagery while considering greenness and wetness based on Tasseled Cap transformation, *Rem. Sens.* 14 (13) (2022) 3001.
- [58] A. Tariq, Y. Jiango, Q. Li, J. Gao, L. Lu, W. Soufan, K.F. Almutairi, M. Habib-ur-Rahman, Modelling, mapping and monitoring of forest cover changes, using support vector machine, kernel logistic regression and naive bayes tree models with optical remote sensing data, *Heliyon* 9 (2) (2023), e13212.
- [59] Y. Huang, J. Peng, N. Chen, W. Sun, Q. Du, K. Ren, Huang K. , Cross-scene wetland mapping on hyperspectral remote sensing images using adversarial domain adaptation network, *ISPRS Journal of Photogrammetry and Remote Sensing* 203 (2023) 37–54.
- [60] J. Liang, C. Chen, Y. Song, W. Sun, G. Yang, Long-term mapping of land use and cover changes using Landsat images on the Google Earth Engine Cloud Platform in bay area-A case study of Hangzhou Bay, China, *Sustainable Horizons* 7 (2023), 100061.
- [61] C. Chen, Y. Chen, H. Jin, L. Chen, Z. Liu, H. Sun, J. Hong, H. Wang, S. Fang, X. Zhang, 3D model construction and ecological environment investigation on a regional scale using UAV remote sensing, *Intelligent Automation & Soft Computing* 37 (2023) 1655–1672.
- [62] B.D. Goffin, R. Thakur, S.D.C. Carlos, D. Srsic, C. Williams, K. Ross, F. Neira-Román, C.C. Cortés-Monroy, Lakshmi, V. Leveraging, remotely-sensed vegetation indices to evaluate crop coefficients and actual irrigation requirements in the water-stressed Maipo River Basin of Central Chile, *Sustainable Horizons* 4 (2022), 100039.
- [63] C. Chen, L. Wang, G. Yang, W. Sun, Y. Song, Mapping of ecological environment based on Google earth engine cloud computing platform and landsat long-term data: a case study of the zhoushan archipelago, *Rem. Sens.* 15 (16) (2023) 4072.